Research Article
P-ISSN: 2971-785X, E-ISSN: 3141-4095
NIGERIAN JOURNAL OF ENGINEERING RESEARCH UNICROSS (NJERU)
DOI: https://doi.org/10.67571/njeru.2026.012935
Volume 3, Issue 1, 26 May 2026, 29-35

Thermal Modelling and Experimental Validation of a 1.5 kW Three-Phase Squirrel-Cage Induction Motor Considering Magnetic Saturation

Onwe Peter Daffin [a], Okoro Ogbonnaya Inya [b], Akpama Eko James [c]

[a] Department of Electrical and Electronic Engineering, University of Calabar, Nigeria.
[b] Department of Electrical and Electronic Engineering, Micheal Okpara University of Agriculture, Nigeria.
[c] Department of Electrical and Electronic Engineering, University of Cross River State, Calabar, Nigeria.

[*]Corresponding author: peteronwe@unical.edu.ng

Received: 24th January, 2026 Revised: 24nd April, 2026 Accepted: 10th May, 2026

ABSTRACT
Temperature rise is one of the major factors limiting the performance, efficiency, and service life of squirrel-cage induction motors. This study presents a transient thermal model of a 1.5 kW three-phase squirrel-cage induction motor, with particular attention to the influence of magnetic saturation on temperature distribution. The model combines electromagnetic loss calculation with a lumped parameter thermal network implemented in ANSYS Motor-CAD. The predicted temperatures were analysed in MATLAB and validated experimentally under rated operating conditions. The results show that the stator winding experiences the highest temperature because of dominant copper losses, while the housing remains the coolest component owing to effective heat dissipation. Incorporating magnetic saturation significantly increases the temperatures of the stator winding, stator core, rotor components, and housing, indicating higher thermal loading under saturated operating conditions. Comparison of the simulated and experimental results shows good agreement, with percentage differences of 9.41%, 13.21%, and 8.35% for the housing, stator back iron, and rotor back iron, respectively. These findings demonstrate that magnetic saturation has a significant influence on the thermal behaviour of induction motors and that the proposed modelling approach provides an effective tool for predicting temperature distribution and supporting the thermal design and performance evaluation of electrical machines.

Keywords— *Squirrel-cage induction motor, finite element analysis, Motor-CAD, Magnetic saturation, electromagnetic torque, experimental validation, MATLAB.*

I. INTRODUCTION

Thermal modelling of squirrel-cage induction motors has evolved from simplified analytical approaches to integrated electromagnetic–thermal models capable of predicting temperature distribution with improved accuracy. Among the available techniques, the lumped parameter thermal network (LPTN) has gained wide acceptance because it provides a good balance between computational efficiency and prediction accuracy. Early studies by Okoro [1] demonstrated the capability of LPTN models to estimate both transient and steady-state temperatures in induction motors. Subsequent investigations by Ejiofor et al. [3, 6] further improved these models by incorporating detailed loss calculations, confirming that stator copper losses are the dominant contributor to temperature rise. Similarly, Afrah and Amer [2] showed that combining Motor-CAD with MATLAB enhances the analysis and interpretation of thermal behaviour.

To improve the estimation of heat generation, several researchers have coupled thermal models with finite element electromagnetic analysis. Abunike et al. [7] applied finite element analysis to predict magnetic flux distribution and associated losses with greater accuracy. Mezani et al. [9] developed a coupled electromagnetic–thermal model that accounted for the interaction between electromagnetic losses and heat transfer, while Ahmed and Kar [8] demonstrated that end-winding regions of totally enclosed fan-cooled induction motors experience significant thermal stress. These studies established that accurate prediction of electromagnetic losses is essential for reliable thermal analysis.

Recent investigations have focused on incorporating nonlinear magnetic characteristics and advanced cooling techniques into thermal models. Laïssaoui et al. [15] included magnetic saturation effects in dynamic induction motor models, showing that nonlinear magnetic behaviour significantly influences loss generation and temperature rise. Hybrid modelling approaches integrating lumped parameter thermal networks with computational fluid dynamics have also been reported by Voigdlener et al. [10] and Nategh et al. [16] to improve cooling analysis. Reviews by Madhavan et al. [17] and Konda et al. [18] further highlighted the importance of enhanced cooling strategies in improving motor efficiency and extending service life.

Experimental validation remains an essential step in assessing the reliability of thermal models. Studies by Ulu et al. [11], Iordache et al. [12], and Kuria and Hwang [13] demonstrated that validated electromagnetic–thermal models provide dependable predictions for machine design and performance evaluation. Akpama et al. [4, 5] further showed that operating conditions such as voltage imbalance and control strategies significantly influence loss distribution and thermal behaviour, emphasizing the need for coupled modelling approaches capable of representing practical operating conditions.

Although considerable progress has been made in thermal modelling of induction motors, many existing studies either employ computationally intensive multiphysics methods or simplify the interaction between electromagnetic losses and heat transfer. Furthermore, relatively few investigations have examined the influence of magnetic saturation on transient temperature distribution while validating the predicted temperatures experimentally. This study addresses these limitations by developing and experimentally validating a transient lumped parameter thermal model of a 1.5 kW squirrel-cage induction motor using ANSYS Motor-CAD. The proposed approach combines electromagnetic loss calculation with thermal network analysis to provide an efficient and accurate prediction of temperature distribution under conventional and saturated operating conditions.

II. METHODOLOGY

A. Mathematical Modelling

The electromagnetic behaviour of the three-phase squirrel-cage induction motor was represented using the conventional dq-axis dynamic model in the synchronous reference frame. The model was employed in ANSYS Motor-CAD to compute electromagnetic quantities, including magnetic flux distribution, torque, and loss components required for thermal analysis. Since the dq formulation is well established in the literature, the complete derivation is omitted for brevity.

The rotor dynamics are governed by

$$J\frac{d\omega_r}{dt} = T_e - T_L - T_B \quad (1)$$

where J is the rotor inertia, T_e is the electromagnetic torque, T_L is the load torque, and T_B represents friction and windage torque.

The heat conduction equation describes the thermal behaviour of the machine

$$\rho c\frac{\partial T}{\partial t} = \nabla \cdot (k\nabla T) + Q \quad (2)$$

where ρ is the material density (kg/m³), c is the specific heat capacity (J/kg·K), T is the temperature (°C or K), t is time(s), k is thermal conductivity (W/m·K), ∇ is the vector differential (gradient/divergence) operator, Q is the volumetric heat generation rate (W/m³)

The motor was modelled using a lumped parameter thermal network (LPTN), in which thermal resistances are given by

$$R_{th} = \frac{L}{kA} \quad (3)$$

where R_{th} is the thermal resistance (K/W), L is the heat conduction path length (m), k is the thermal conductivity of the material (W/m·K), A is the cross-sectional area normal to heat flow (m²)

Total heat generation is given by:

$$Q = P_{cu} + P_{core} + P_{mech} \quad (4)$$

where Q is total heat generated within the motor (W), P_{cu} is the stator copper loss (W), P_{core} is the core (iron) loss due to hysteresis and eddy currents (W), P_{mech} is the mechanical loss due to friction and windage

with stator copper losses calculated as

$$P_{cu} = 3I^2R_0[1 + \alpha(T - T_0)] \quad (5)$$

where P_{cu} is three-phase stator copper loss (W), I is phase current (A), R_0 is the stator winding resistance at the reference temperature T_0(Ω), α is the temperature coefficient of resistance for copper ($°C^{-1}$), T is the operating winding temperature (°C), T_0 is the reference temperature (°C)

Equations (1)–(5) constitute the coupled electromagnetic–thermal model implemented in ANSYS Motor-CAD to predict the steady-state temperature distribution of the induction motor.

B. *Thermal–Magnetic Saturation Assessment*

To determine whether magnetic saturation influences the thermal performance of the induction motor, two operating conditions were considered: the reference condition at 380 V, 50 Hz and an increased excitation condition at 420 V, 50 Hz. The machine geometry and supply frequency were kept constant, while the nonlinear B–H characteristic of the M350-50A electrical steel was incorporated into the finite-element electromagnetic model. Since the supply frequency remained unchanged, increasing the voltage increased the magnetic excitation and flux level within the machine, thereby providing a basis for assessing the effect of magnetic saturation on electromagnetic losses and temperature rise.

The electromagnetic losses obtained from each operating condition were subsequently transferred to the thermal model as heat sources. The resulting temperature distributions and transient thermal responses were then compared to determine how the increased magnetic excitation affected the thermal behaviour of the machine.

The motor parameters used for this work are:

TABLE I
MOTOR SPECIFICATION AND GEOMETRY

Parameters	Value
Rated power	1.5 kW
Rated voltage	380 V
Rated current	3.83 A
Rated speed	1390 rpm
Frequency	50 Hz
Pole number	4
Slot number	24
Stator lamination diameter	170mm
Stator bore	98.6mm
Tooth width	10mm
Rotor bars	34
Slot depth	25mm
Yoke thickness	12mm
Airgap	1mm
Shaft diameter	28mm
Rotor diameter	96.6mm
Rotor tooth width	4mm
Bar opening	1.5mm
Bar depth	10mm

The parameters in Table 1 were used as input data for developing the electromagnetic finite element model in Motor-CAD, which is used to compute the magnetic field distribution, electromagnetic torque, and associated losses of the machine.

III. RESULTS AND DISCUSSIONS

A. *Transient Thermal Response under Rated Load Condition*

Figures 1 and 2 show the thermal response of the induction motor under rated load operation. The temperatures of all components rise rapidly at the start of the simulation before gradually reaching steady-state after about 40 minutes. This indicates that the heat generated within the motor is balanced by the heat dissipated to the surroundings.

The stator winding reaches the highest temperature (80.54°C), confirming that it is the main source of heat due to copper losses. The stator back iron stabilizes at 62.38°C, while the rotor back iron and rotor bars reach about 51.5°C, indicating lower heat generation in the rotor. The housing records the lowest temperature (47.29°C) because it dissipates heat directly to the surrounding air.

These results show that, under no-load conditions, the stator winding is the most thermally stressed part of the motor, while the cooling system effectively limits the temperature rise of the housing. The smooth temperature profiles also indicate stable thermal behaviour throughout the simulation.

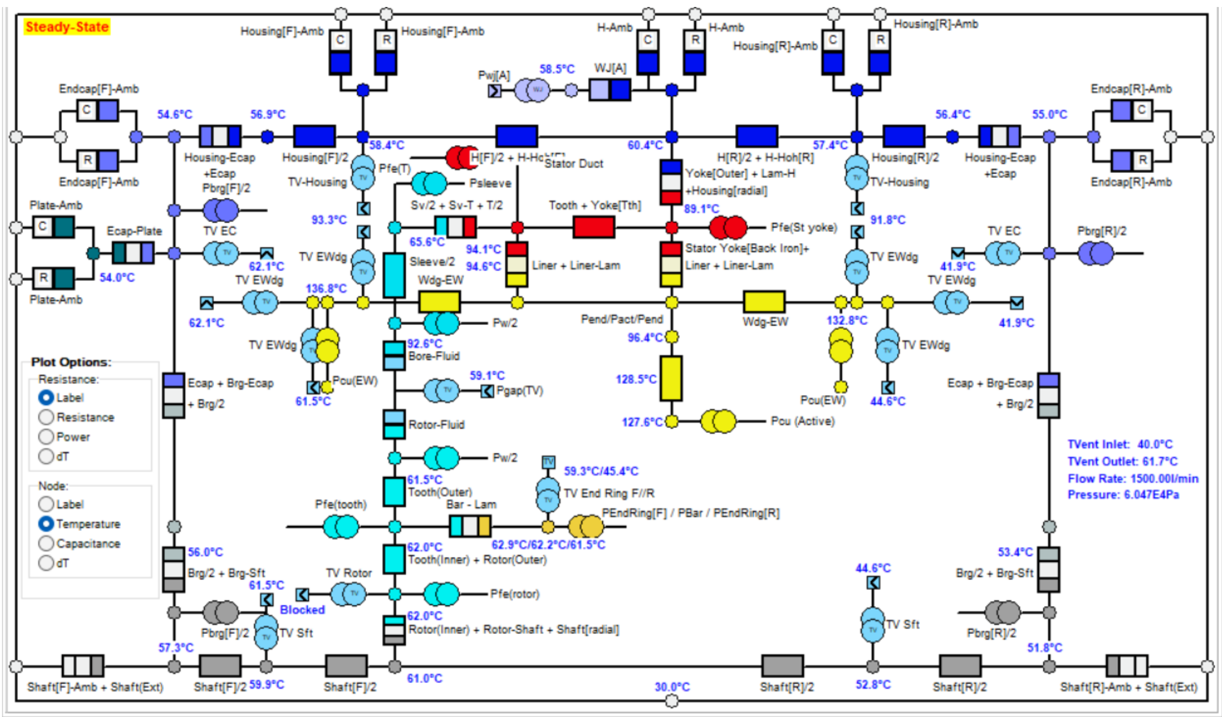

FIGURE 1: TRANSIENT TEMPERATURE SCHEMATIC WITH MAGNETIC SATURATION

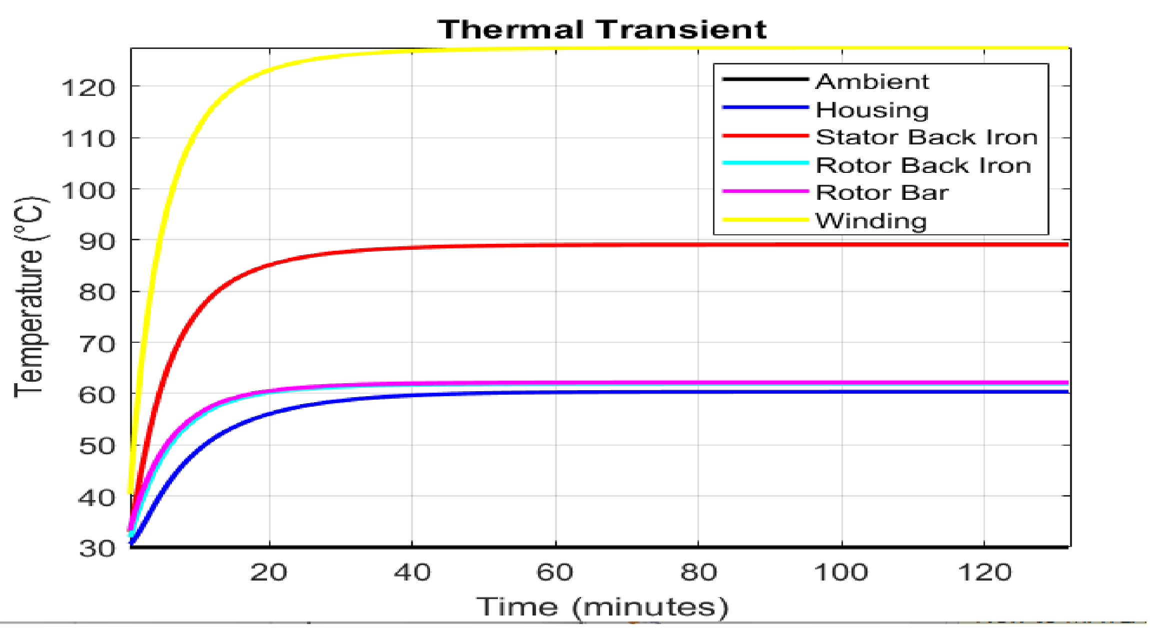

FIGURE 2: TRANSIENT TEMPERATURE DISTRIBUTION WITH MAGNETIC SATURATION

B. Comparison between rated load and magnetic saturation

The comparison shows that the increased magnetic saturation condition produced higher steady-state temperatures in all the major components of the motor when compared with the rated-load condition.

The winding recorded the highest temperature increase, rising from approximately 80°C at rated load to 126°C under the magnetic saturation condition. This represents a temperature difference of 46°C and a percentage increase of 57.50%.

The stator back iron temperature increased from approximately 62°C to 90°C, giving a difference of 28°C, equivalent to a 45.16% increase. The housing temperature increased by approximately 13°C, from 47°C to 60°C, while the rotor back iron also increased by approximately 13°C, from 51°C to 64°C.

the results indicate that operating the motor under increased magnetic excitation significantly increases its thermal response. The winding is the most affected component, followed by the stator back iron. This suggests that magnetic saturation has a considerable effect on the internal heat generation and temperature distribution within the motor.

TABLE II
COMPARISON OF RATED-LOAD AND MAGNETIC-SATURATION THERMAL RESPONSES

Motor Component	Rated Load Temperature (°C)	Magnetic Saturation Temperature (°C)	Difference (°C)	Percentage Difference (%)
Ambient	30	30	0	0.00
Housing	47	60	13	27.66
Stator Back Iron	62	90	28	45.16
Rotor Back Iron	51	64	13	25.49
Winding	80	126	46	57.50

C. Experimentation

Experimental validation was carried out to evaluate the accuracy of the proposed thermal model under rated operating conditions. The test motor was a 1.5 kW, three-phase squirrel-cage induction motor rated at 380 V, 50 Hz, and 3.83 A with Class F insulation. The supply voltage was varied from no-load to rated voltage using a three-phase variac. Electrical quantities and rotor speed were measured using standard laboratory instruments, while temperatures at the motor housing, stator surface, and rotor surface were measured with a non-contact infrared thermometer after thermal steady-state was reached. The ambient temperature was maintained at approximately 30°C throughout the tests. The experimental setup is shown in Figure 5, while the measured results are presented in Table 3.

These measurements were used directly for comparison with the corresponding Motor-CAD results.

The experimental measurements are presented in table 3:

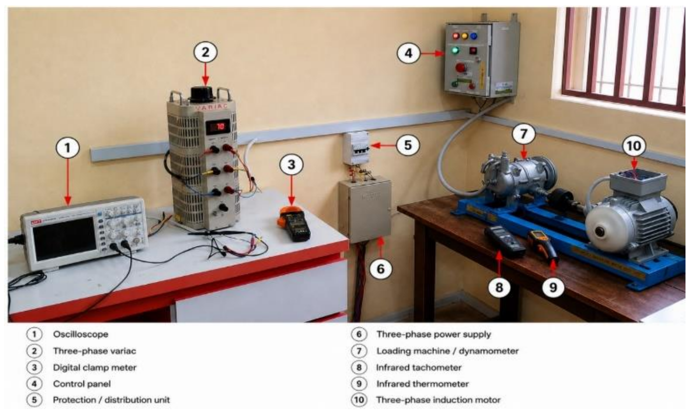

FIGURE 3. EXPERIMENTAL SETUP USED FOR THERMAL VALIDATION

TABLE III
EXPERIMENTAL MEASUREMENT OF THE MOTOR AT RATED LOAD

S/No	Temperature	Values	Unit
1	Ambient	30	°C
2	Housing	52.2	°C
3	Stator back iron	55.1	°C
4	Rotor back iron	56.2	°C

D. Comparison of simulation and experimental Results

Table 4 compares the simulated and measured temperatures of the induction motor at rated load. The results show good agreement between the two sets of data. Percentage differences of 9.41%, 13.21%, and 8.35% were obtained for the housing, stator back iron, and rotor back iron, respectively. The largest deviation occurred in the stator back iron, which is likely due to simplified heat transfer assumptions and uncertainties associated with the experimental measurements.

The simulated temperatures are generally close to the measured values, indicating that the proposed thermal model predicts the motor temperature distribution with satisfactory accuracy. Experimental measurements of the stator winding and rotor bar temperatures were not possible because these components are inaccessible during normal operation. Nevertheless, the agreement obtained for the accessible components confirms the suitability of the model for thermal analysis and performance evaluation.

TABLE IV
COMPARISON OF MEASURED AND SIMULATED TEMPERATURES AT RATED LOAD

Motor Components	**Measured (°C)**	**Simulated (°C)**	**Difference**
Housing	52.2 °C	47.29°C	9.41%
Stator back iron	55.1 °C	62.38°C	13.2%
Rotor back iron	56.2 °C	51.51°C	8.35%
Rotor bar average	N/A	51.67°C	
Winding	N/A	80.54°C	

N/A indicates that the temperature could not be measured experimentally because the component was inaccessible during operation.

IV. CONCLUSIONS

The Temperature rise is an important factor in the performance and service life of squirrel-cage induction motors. This study investigates the transient thermal behaviour of a 1.5 kW three-phase squirrel-cage induction motor, with attention given to the effect of increased magnetic excitation on temperature distribution. The study was carried out using ANSYS Motor-CAD, where the electromagnetic losses were used as heat sources for the thermal model. MATLAB was also used for further analysis of the results. Experimental temperature measurements were taken under the rated operating condition to compare with the simulation results. Two operating conditions were considered. The first was the rated operating condition at 380 V and 50 Hz, while the second involved increasing the voltage to 420 V while maintaining the frequency at 50 Hz. The increase in voltage increased the magnetic excitation of the motor and moved the magnetic circuit closer to saturation. The results showed that the stator winding had the highest temperature under both operating conditions. At the rated condition, the winding temperature was approximately 80.5°C, while at the increased-voltage condition, it rose to about 127°C. The temperatures of the stator back iron, rotor back iron, and housing also increased.

The simulated temperatures were compared with experimental measurements at accessible locations on the motor. Percentage differences of 9.41%, 13.21%, and 8.35% were obtained for the housing, stator back iron, and rotor back iron, respectively. The results show that increased magnetic excitation can lead to higher internal heat generation and a corresponding rise in motor temperature. The study shows that increased magnetic excitation has a noticeable effect on the temperature distribution of an induction motor. The results also show that the coupled electromagnetic and thermal approach used in this study can be useful for examining the thermal behaviour of the motor under different operating conditions.

AI DISCLOSURE STATEMENT.

The author(s) used ChatGPT (OpenAI) during the preparation of this manuscript to assist with language editing, improving clarity of the manuscript. The author(s) reviewed and edited the content as necessary and take full responsibility for the final version of the work.

References

[1] O. I. Okoro, “Steady and transient states thermal analysis of a 7.5-kW squirrel-cage induction machine at rated-load operation,” *IEEE Transactions on Energy Conversion*, vol. 20, no. 4, pp. 730–735, 2005.

[2] T. A. Afrah and A. M. Amer, “Thermal analysis of a three-phase induction motor based on Motor-CAD, Flux2D and MATLAB,” *Indonesian Journal of Electrical Engineering and Computer Science*, vol. 15, no. 1, pp. 46–53, 2019.

[3] O. S. Ejiofor, C. Awah, C. Nnonyelu, and O. I. Okoro, “Thermal modelling and analysis of a 10 HP induction machine using the lumped parameter approach,” *International Journal of Integrated Engineering*, vol. 13, no. 6, 2021.

[4] E. J. Akpama, O. I. Okoro, and E. Chikuni, “Simulation of the performance of induction machine under unbalanced source voltage

conditions," *Pacific Journal of Science and Technology*, vol. 11, no. 1, pp. 9–15, 2010.

[5] E. J. Akpama, I. E. Omini, E. E. Effiong, and R. U. Ezenwosu, "PID speed controlled model of induction motor using Simulink," *International Journal of Engineering Research and Management*, vol. 7, no. 10, pp. 24–28, 2020.

[6] E. C. Abunike, O. I. Okoro, and G. D. Umoh, "Steady and dynamic states analysis of induction motor: FEA approach," *Nigerian Journal of Technology*, vol. 36, no. 4, pp. 1202–1207, 2017.

[7] F. Ahmed and N. C. Kar, "Analysis of end-winding thermal effects in a totally enclosed fan-cooled induction motor with die-cast copper rotor," *IEEE Transactions on Industry Applications*, vol. 53, no. 1, pp. 50–60, 2017.

[8] S. Mezani, N. Takorabet, and B. Laporte, "A combined electromagnetic and thermal analysis of induction motors," *IEEE Transactions on Magnetics*, vol. 41, no. 5, pp. 1572–1575, 2005.

[9] T. Voigdlener, D. Jochelavicius, and M. A. Peretti, "Thermal analysis of an induction motor by hybrid modeling of a thermal equivalent circuit and CFD," *IEEE Transactions on Industrial Electronics*, vol. 66, no. 3, pp. 2272–2280, 2019.

[10] C. Ulu, O. Korman, and G. Kömürgöz, "Electromagnetic and thermal analysis/design of an induction motor for electric vehicles," *International Journal of Mechanical Engineering and Robotics Research*, vol. 7, no. 6, 2018.

[11] M. Iordache, L. Dumitriu, D. Niculae, N. Galan, S. Deleanu, and L. Mandache, "Dynamic performance analysis of deep bars squirrel cage induction motor by simulation," *Annals of the University of Craiova, Electrical Engineering Series*, vol. 37, pp. 45–52, 2013.

[12] J. Kuria and P. Hwang, "Investigation of thermal performance of electric vehicle BLDC motor," *International Journal of Mechanical Engineering*, vol. 1, no. 1, pp. 1–17, 2012.

[13] P. D. Onwe, E. J. Akpama, O. I. Okoro, and O. Ekpenyong, "Dynamic behavior of asynchronous motor under balanced and unbalanced voltage source conditions," *World Journal of Engineering Research and Technology*, vol. 11, no. 4, pp. 239–252, 2025.

[14] M. Laïssaoui, M. R. Mékidèche, D. Sedira, and A. Ladjimi, "Dynamic modeling of induction motor taking into account thermal stresses," *COMPEL: The International Journal for Computation and Mathematics in Electrical and Electronic Engineering*, vol. 26, no. 1, pp. 139–150, 2007.

[15] S. Nategh, Z. Huang, A. Krings, O. Wallmark, and M. Leksell, "Thermal modeling of directly cooled electric machines using lumped parameter and limited CFD analysis," *IEEE Transactions on Energy Conversion*, vol. 28, no. 4, 2013.

[16] S. Madhavan, R. P. B. Devdatta, E. Gundabattini, and A. Mystkowski, "Thermal analysis and heat management strategies for an induction motor: A review," *Energies*, vol. 15, Art. no. 8127, 2022.

[17] Y. R. Konda *et al*., "Thermal analysis and cooling strategies of high-efficiency three-phase squirrel-cage induction motors—A review," *Computation*, vol. 12, no. 1, Art. no. 6, 2024.

[18] J. Mróz, "The model of a double-cage induction motor for the analysis of thermal fields in transient operations," *Archives of Electrical Engineering*, vol. 66, no. 2, pp. 397–408, 2017.